First-principles calculations of liquid CdTe at temperatures above and below the melting point

Vitaliy V. Godlevsky, Manish Jain, Jeffrey J. Derby, and James R. Chelikowsky
Department of Chemical Engineering and Materials Science, Minnesota Supercomputing Institute, University of Minnesota, Minneapolis, Minnesota 55455
(Received 5 February 1999)

We perform *ab initio* molecular-dynamics simulations of CdTe at three different temperatures: 800 K (supercooled state), 1370 K (near the melting temperature), and 3000 K (superheated state). In agreement with experiment, we find that upon the melting, CdTe experiences a semiconductor→semiconductor transition. In its liquid state, CdTe retains its tetrahedral environment with the coordination number ~4. We find that heating CdTe much above its melting point leads to substantial structural changes with a transformation to a more close-packed atomic structure. The coordination number of the superheated phase is ~6 and the dc electrical conductivity is an order of magnitude larger than at the melting temperature. This, along with the disappearance of the finite band gap, suggests a gradual semiconductor→metal transition in the CdTe system at a temperature higher than melting point. We also find in liquid CdTe, near the melting temperature, atoms of Te form infinite branched chains. Short and simplified chains are still present in the supercooled phase. As the temperature increases, chains break, become shorter, and, eventually, transform to form close-packed clusters in the supeheated state. We also examine dynamical and electronic properties of the CdTe system.
[S0163-1829(99)15635-2]

I. INTRODUCTION

With the advent of powerful computational tools and algorithms, *ab initio* molecular dynamics simulations have become a popular instrument for studying disordered materials. Liquid and amorphous semiconductors are among such systems. Group-IV semiconductors, such as Si and Ge, have been favorite subjects of such studies and have received broad attention in the past decade. Numerous first-principles simulations of amorphous, molten, and even superheated states exist for these semiconductors.[1–5] A range of liquid and amorphous III–V semiconductors has also been examined recently. First-principles simulations of such materials as GaAs, GaSb, and InP,[6–8] have been carried out. However, there have been only a few experiments examining structural properties of II–VI materials in the molten state[9,10] and no first-principles simulations to our knowledge.

Among II–VI semiconductors, CdTe is of special technological interest. Cadmium telluride and its alloys are employed to fabricate a wide array of electro-optic devices, high-performance infrared detectors, and room-temperature radiation detectors. For example, infrared sensors based on epitaxial layers of $Hg_{1-x}Cd_xTe$ (HgCdTe) typically are grown on single-crystal CdTe substrate. In order to continue the advance of such applications, large, high-quality single crystals of CdTe are required. However, the growth of such material has proven to be extremely difficult.[11,12] These difficulties have motivated growth experiments in the microgravity environment of earth orbit.[13] A more complete understanding of the physics of the melt state should provide important information to solve the technical difficulties of CdTe growth.

Besides being a technologically important compound, liquid CdTe (*l*-CdTe) also presents an interesting subject for fundamental studies.[14] CdTe is among those II–VI semiconductors that, in the liquid phase, exhibit properties which are quite different from those of liquid IV and III-V semiconductors. In particular, neutron-scattering experiments[9,10] suggest that liquid CdTe conserves its crystalline open structure environment with the coordination number of ~4. An empirical rule formulated by Joffe and Regel[15] states that a molten or amorphous semiconductor retains its semiconductor properties, despite the destruction of long-range order, *only* if the short-range order of the crystalline phase is preserved. Indeed, though its electrical conductivity value undergoes a jump by an order of magnitude during melting, *l*-CdTe remains a semiconductor in the melt: Its electrical conductivity *increases* with temperature.

This is in contrast with IV and III-V compounds. These semiconductors become more close packed in the liquid phase with the coordination number increasing to ~6.[4–7] In the melt, these materials experience a relative volume contraction up to 13%.[16] It is believed that structural changes occurring in the melting process result in the disruption of covalent bonds and a partial delocalization of electrons. This leads to a semiconductor→metal transition.[16] In our study of CdTe, we fixed the density of the liquid to that measured at the melting point. This has the advantage of focusing on temperature changes alone. One might assume an increase in density if the liquid undergoes a fourfold to sixfold structure transformation. But this is a relatively small change and it is not obvious that the coordination change will be reflected in a density change in the liquid state. For example, we find that upon melting, CdTe does not change the nearest-neighbor coordination despite a 9% decrease in volume. Moreover, in previous studies for III-V's, we have altered the volume by $\pm 10\%$ and found very small changes on the structure of the liquid. This is consistent with studies on metallic liquids.[17]

Another significant difference in the local order between CdTe and III-V semiconductors is the dissociation degree of anion-cation bonds. Following simple thermodynamic estimates,[19] the curvature of the liquidus can be expressed as

a function of the entropy change in the solid-liquid transition and the dissociation degree of anion-cation bonds in the liquid phase. In contrast to III-V materials, the phase diagram of CdTe has a sharp hyperbolic liquidus at the congruent point.[18] This implies that *l*-CdTe has a significant number of heterogeneous bonds conserved,[20] i.e., in *l*-CdTe, the cation tends to exist within a tetrahedral configuration of anions and vice versa. This conservation of local order in *l*-CdTe serves to verify the Joffe-Regel rule.[15] Conversely, for the liquid III-V compounds, the local environment is significantly altered. In addition to the increase of the coordination number, the stoichiometry of the bonds is changed. For instance, in *l*-GaAs, dissipation of heteropolar bonds is substantial.[20] The first coordination shell consists of $\sim$50% of atoms of the same species as the reference atom.[21]

The assumption that CdTe has more crystalline structural attributes preserved in the melt (compared to liquid III-V semiconductors) is reinforced by a low entropy change for the solid→liquid phase transition observed in the experiment.[22] Tetrahedral and compositional order in the local environment of *l*-CdTe has lower entropy than a sixfold structure of liquid III-V materials with a higher concentration of stoichiometric defects (or ''wrong bond'' defects, which are absent in the crystalline phase of the semiconductor).

The semiconductor behavior of *l*-CdTe is observed only in a narrow temperature range immediately after melting temperature. Upon further heating, at the temperature $\sim$120 K higher than the melting point, electrical conductivity of *l*-CdTe experiences a sharp increase and the liquid phase becomes metallic.[16] Gaspard *et al.*[10] proposed that *l*-CdTe undergoes fourfold→sixfold transformation under higher temperature. This would explain the metallic behavior of the melt. Also, Glazov *et al.*[16] made a hypothesis that atomic chains are an essential feature of *l*-CdTe. If such chains exist in the liquid, they could be a partial explanation for the difficulty in growing a pure single crystal from a liquid phase. Here we confirm that atoms of Te form helicon chains in the melt. To investigate the structural properties of the melt and the behavior of chains above and below the melting point, we will consider three different temperature regimes: one at the melting point (1370 K), one considerably below the melting (800 K), and one considerably above the melting point (3000 K).

II. COMPUTATIONAL METHODS

II-VI semiconductors containing group-IIB elements can present severe computational challenges in computing their electronic structure. In our work, we use pseudopotentials to describe the ion-electron interactions. Pseudopotentials have great advantages over all-electron methods as one needs only to solve for the valence electrons. Unfortunately, for IIB elements, it is not clear whether the filled *d* orbitals can be treated as core electrons. Often, these shells cannot be considered as chemically inert as they possess significant overlap with the *s* valence electrons and cannot be neglected in describing the structurual properties of II-VI semiconductors. On the other hand, treating *d* electrons as a valence shell dramatically increases the complexity of the problem. First, the number of valence electrons would increase from 8 to 18 per anion-cation pair. This more than doubles the number of required eigenvalues. Second, the *d* potential corresponding to the filled shell is much stronger and more localized than the empty shell potential. Consequently, more plane waves are required for equivalently converged eigenvalues.

TABLE I. Lattice constants and bulk moduli for zinc-blende phase of CdTe calculated with different Cd potentials. The cutoff radii used to generate Cd potentials are also listed.

	a (Å)	B (GPa)	r_c (for $s/p/d$ in Å)
$Cd^{2+}5s^25p^05d^0$	6.13	51	1.38/1.38/1.90
$Cd^{2+}5s^25p^05d^0$ Partial core correction	6.43	43	1.38/1.38/1.90
$Cd^{12+}4d^{10}5s^25p^0$	6.45	47	1.38/1.27/1.69
Experiment	6.48	42 (Ref. 38) 44 (Ref. 39)	

Fortunately, this problem can be addressed via a ''partial-core'' pseudopotential scheme.[23] In this scheme, the *d* electrons are considered as part of the core. Each time the exchange-correlation term is calculated for a self-consistent field calculation, a fixed *d*-core charge density is added to the valence charge density. We followed the method of Troullier-Martins[24] to generate *ab initio* pseudopotentials using Ceperly-Alder correlation.[25] The nonlocal part of the pseudopotentials is taken to be in the Kleinman and Bylander[26] factorized form.

We tested three different pseudopotentials of Cd: one with the $4d$ electrons treated as core states, one with $4d$ core electrons plus a partial core correction scheme, and one with $4d$ electrons as part of the valence shell. We examined these potentials by calculating the crystalline properties of CdTe. We used 30 Ry as the cutoff energy. The Brillouin zone for a two atom primitive cell was sampled by 10 irreducible *k* points. Table I summarizes our results and gives the Cd pseudopotential parameters. The pseudopotentials for Te employed core radii of 1.38/1.27/1.53 (in Å) for $s/p/d$ potentials, respectively. We generated the potentials with *p* local components for both atoms.

The pseudopotential with the $4d$ electrons omitted results in a substantially underestimated lattice constant and overestimated bulk modulus. The partial core correction scheme results in a noticeable improvement. The partial core pseudopotental yields a lattice constant within 1% accuracy compared to the experiment value and a bulk modulus within 2% accuracy. The results of the partial core potential are within ''computational'' error to those of the pseudopotential, which includes the $4d$ as part of the valence shell. In Fig. 1, we compare band structures obtained with two different potentials: one for Cd^{12+} and one for Cd^{2+} constructed with core correction.[23] Cd $4d$ electrons form a narrow, 1.5 eV, band. The agreement between the two band structures is excellent for *p* electrons at the top of the valence band and for the conductivity band. This is important, because we will need to evaluate dipole transitions between these two bands to calculate optical conductivity. The presence of the $4d$ band shifts the Te *s* band (the lowest valence band in CdTe) by 1.5 eV. The Te *s* band is a ''semicore'' state as it resides

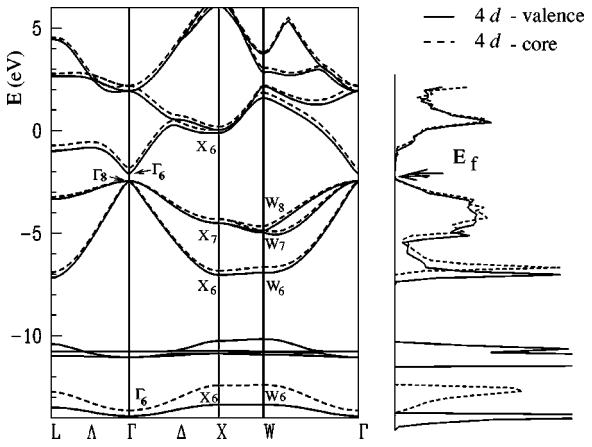

FIG. 1. Band structure (left panel) and density of states (right panel) for CdTe. Two calcuations are shown. The solid lines show results where the $4d$ electrons are treated as valence electrons. The dashed lines show results where the $4d$ electrons are included in the core using a partial core correction scheme (see text).

over 10 eV below the top of the valence band. As such, its precise placement is not crucial in determining the band configuration near the gap.

Another test we performed to validate the usage of the core-corrected pseudopotential was to compare the dynamical properties of the liquid with and without the $4d$ states. We ran a molecular-dynamics simulation for a small system of eight atoms within a supercell for 3 ps. We found no significant difference between the two potentials in the trajectories of the atoms. The largest difference in the final positions of the atoms was less than a few percent of the net distance traveled in the simulation. We view these comparisons as validating our use of the partial core correction.

We model l-CdTe by a supercell with periodic boundary conditions. There are 64 atoms in the system. The size of the cubic supercell corresponds to $2a$, where a is a lattice parameter of the conventional fcc cell of the crystalline phase; a is chosen to agree with the experimental density of l-CdTe at the melting temperature, $\rho = 5.64\ \ g/\mathrm{cm}^3$.[18] The system of 64 atoms per unit cell should be large enough for liquid semiconductor simulations.[1–5] The structure of the liquids lacks long-range correlation. As will be shown in the next section, this is also the case with l-CdTe. The pair distribution of the molten phase attenuates quite strongly after the first peak, i.e., atoms do not correlate with their images in the periodically replicated neighbor cells.

To prepare a representative ensemble of l-CdTe, we start with a system of 32 atoms of Cd and 32 atoms of Te randomly placed in the cell. We impose the constraint that no two atoms be closer than a specified minimum distance, e.g., less than 90% of the bond length in the crystal. Next, we thermalize the system at a fictive temperature of 6000 K. By thermalizing the system at this ''hot'' temperature, we ensure a proper ''mixing'' of atoms and remove the bias of the system to the initial condition. We believe that starting from a random atomic configuration is better than starting from a perfect crystal system. First, by arranging atoms randomly, a significant energy is imparted into the system, since such a configuration is far from optimized. Dissipation of this energy in the beginning of the simulations helps to activate compositional defects whose formation energies might be large. The random atomic configuration also introduces possible stoichiometric defects. If such defects exist in the liquid, they might be inaccessible for the simulation time implemented if one started from the crystalline structure (typical simulation times for *ab initio* calculations are on the order of several ps for systems of this size). Second, starting from crystalline structure would require the size of the supercell to be a multiple of the primitive or conventional cell size. In our method, the supercell size can be arbitrary. However, in the present work, we follow the conventional 64-atom/cell size to be able to compare our calculations with the previous simulations of liquid IV and III-V semiconductors consistently.

We use Langevin dynamics to prepare the liquid state ensemble.[27,28] The trajectory of each atom is computed from

$$m_i \frac{d\vec{v}_i}{dt} = -\gamma \vec{v}_i + \vec{R}_i(\gamma, T) + \vec{F}_i, \tag{1}$$

where $\vec{F}_i$ is the interatomic force on the ith particle, m_i is the mass of the particle, and γ is the viscosity of the medium. The particles are subject to rapidly varying random forces, $\vec{R}_i(\gamma, T)$. The random forces are a function of temperature and viscosity described by the fluctuation-dissipation theorem.[29] Random forces and viscosity couple the system with the hypothetical heat bath. The time step used in integrating the equation of motion is 300 a.u. (1 a.u. $= 2.4 \times 10^{-17}$ s). The interatomic forces, $\vec{F}_i$, are computed quantum mechanically from the pseudopotential wave functions and the Hellmann-Feynman theorem.[28] We constructed the charge density using the zone-center k point of the supercell. For molecular-dynamics simulations, we used an energy cutoff of 10 Ry.

We simulated CdTe at three different temperatures. Previous work on semiconductor liquids has suggested that the melting points obtained from *ab initio* simulations are in reasonable agreement with experiment, e.g., within a few hundred degrees.[30] Here it is not crucial that we have the precise theoretical melting point replicated in our simulation. Rather, we wish to consider three general temperature regimes: 800 K, 1370 K (the known melting point), and 3000 K. By examining the self-diffusion of (Cd,Te) in the melt, we can verify that these regimes correspond to liquidlike states. For discussion purposes, we will characterize the 800 K simulation as corresponding to a ''supercooled state,'' the 1370 K simulation corresponding to the ''liquid state,'' and the 3000 K simulation corresponding to a ''superheated state'' of the liquid.

To obtain these temperature regimes, we initially thermalize the system at 6000 K using Langevin dynamics for 2 ps. At that time, the average diffusion path of the atoms becomes comparable with the conventional lattice size. We anneal the system for 1 ps to a temperature of 3000 K. To build a representative ensemble of states for superheated CdTe, we run the system for 3 ps at this temperature. Then we anneal the system to the melting temperature of 1370 K during a period of 1 ps. After this, we run the system for 3 ps at this temperature to acquire the statistics for l-CdTe. Then we anneal the liquid to 800 K to form the supercooled state. We performed this procedure gradually during 5 ps. The result-

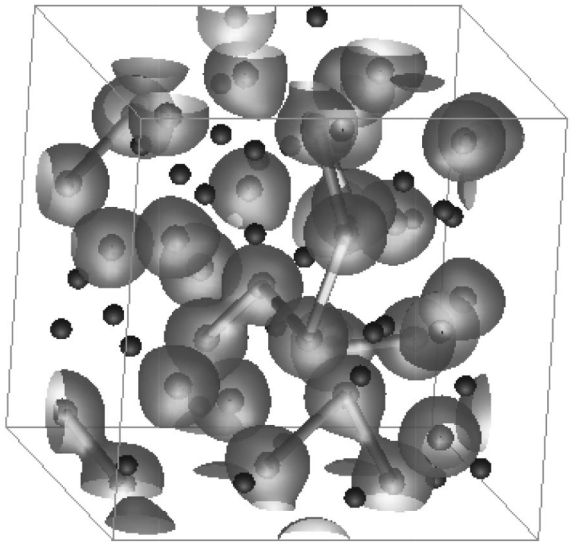

FIG. 2. A snapshot showing a typical *l*-CdTe structure in the supercell (see text). Atoms of Cd are represented by dark spheres, atoms of Te are shown by light spheres.

ing phase is a ''viscous'' liquid; its viscosity is an order of magnitude larger than the corresponding value at the melting temperature.

III. PROPERTIES OF LIQUID CADMIUM TELLURIDE AT DIFFERENT TEMPERATURES

A. Structural properties

In the crystalline phase, the Cd-Te bond has a strong ionic nature, its Phillips ionicity[31] being 0.72. We find that the ionic nature of the material is preserved in the liquid phase. In Fig. 2, we show a typical structure of *l*-CdTe in the supercell. This ''snapshot'' is taken at one of the time steps during 3 ps simulation of *l*-CdTe at 1370 K. We choose to characterize the density by considering an isocharge surface. This surface is defined by a charge density corresponding to one-half of its maximum value in the supercell. Electronic charge-density isosurfaces in supercooled and superheated CdTe are very similar to those presented on the picture. Projection of the wave functions on the partial states shows that Te bonds have pronounced *p*-electron character. Charge-density configurations associated with the Cd cations tend to be *s*-like and localized on the atomic sites.

Using the atomic positions at each time step, and averaging the positions over the representative ensemble, we obtain total pair correlation functions, $g(R)$. For supercooled CdTe, we average $g(R)$ over the last 100 molecular-dynamics (MD) steps, after the system becomes viscous. For *l*-CdTe and superheated CdTe, we average $g(R)$ for the last 300 MD steps (2.2 ps) of the simulations at 1370 K and 3000 K, respectively. Total pair correlation functions are shown in Fig. 3.

For all three temperatures, the first peak has the same coordinate of 2.8 Å. The first shell can be defined by the coordinate of the first minimum, $R_{\min}$. As the temperature increases, this peak becomes wider and its amplitude decreases. This results in a shifting of $R_{\min}$ from $R_{\min}=3.5$ Å (for supercooled Te) to $R_{\min}=3.6$ Å and 4 Å for *l*-CdTe and

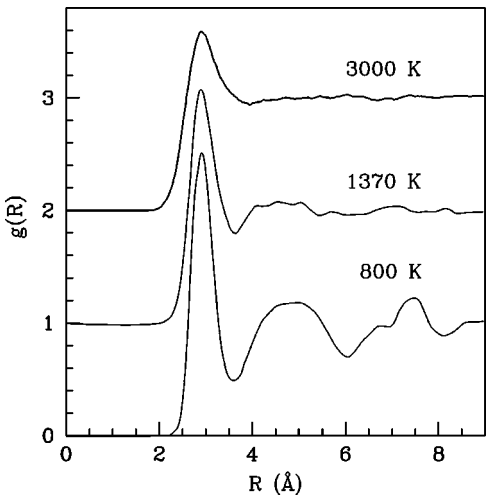

FIG. 3. Total pair correlation functions for liquid CdTe at different temperatures.

superheated CdTe respectively. From the plot, it can be seen that the high temperature destroys long-range correlation. While supercooled CdTe has a well defined first, second, and third shell and *l*-CdTe has well defined first and second shells, the radial distribution function for superheated CdTe becomes ''flat'' immediately after the first peak. We find in all cases that the absence of long-range correlation at the lengths of a (the length of the supercell $a=13.37$ Å) validates *a posteri* the usage of a 64-atom supercell.

To compare our calculations with neutron-scattering experiment, we obtain the total structure function as a linear combination of the partial structure factors, $S_{\mathrm{CdCd}}(q)$, $S_{\mathrm{CdTe}}(q)$, and $S_{\mathrm{TeTe}}(q)$, normalized by the scattering lengths:

$$S(q)=\frac{\alpha_\alpha^2 S_{\alpha\alpha}(q)+2\alpha_\alpha\alpha_\beta S_{\alpha\beta}(q)+\alpha_\beta^2 S_{\beta\beta}(q)}{\alpha_\alpha^2+\alpha_\beta^2}, \quad (2)$$

where the ratio of the scattering lengths[32] is taken to be $\alpha_{\mathrm{Cd}}/\alpha_{\mathrm{Te}}=5.8/7.5$. Partial structure factors are obtained from partial radial distribution functions by a Fourier transformation:

$$S_{\alpha\beta}(q)=\delta_{\alpha\beta}+4\pi\rho_{\alpha\beta}\int_0^\infty [g_{\alpha\beta}-1]\frac{\sin(2\pi qr)}{2\pi qr}r^2 dr, \quad (3)$$

where $\rho_{\alpha\beta}$ is partial density.

In Fig. 4, we show our theoretical total structure factors compared with available experiment[9] and the theoretical results obtained from a molecular-dynamics simulation based on a Stillinger-Weber-type classical potential.[33] For *l*-CdTe, the agreement between theory and experiment is good for the third and fourth peaks at ~ 5 Å and ~ 7.5 Å, respectively. The agreement between our theory and Stillinger-Weber-type calculations is excellent for these two peaks. It suggests that the angular-dependent classical potential reproduces our quantum-mechanical interactions on the short-range scale. Our calculations reasonably reproduce the structure of experimental 1.7 Å and 3.0 Å peaks. As the temperature increases and disorder is introduced, features corresponding to the long-range correlation [first peaks of $S(Q)$] become less

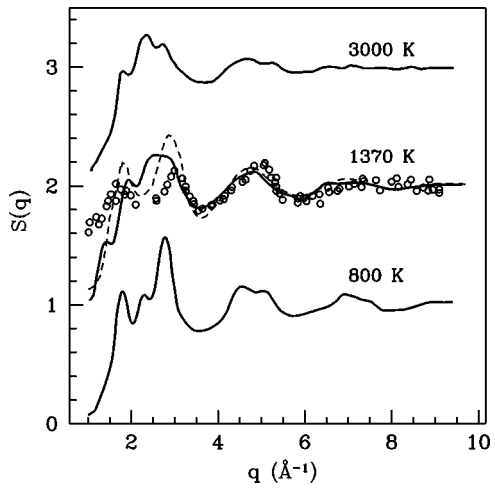

FIG. 4. Total structure factors. For *l*-CdTe at the melting temperature we compare our data with available experiment (Ref. 9) (dots) and the result obtained with Stillinger-Weber potential simulations (Ref. 33) (dashed line).

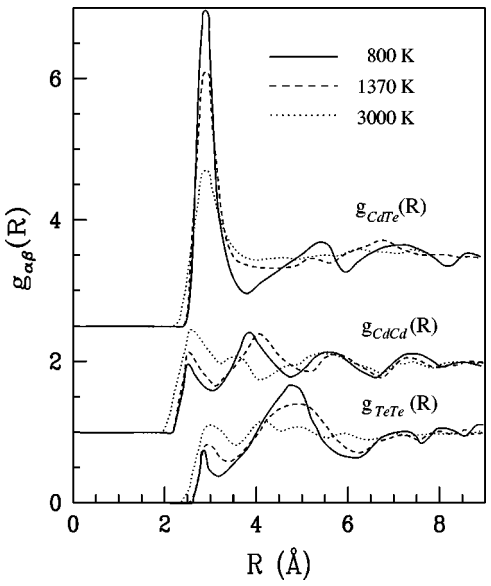

FIG. 5. Partial radial distribution functions, g_{CdTe}, g_{CdCd} and g_{TeTe} (see text).

prominent. As the temperature varies, the second peak also experiences a significant morphological change. At the melting point, *l*-CdTe has a symmetric form of the peak at 2.7 Å. At 3000 K, the peak becomes asymmetric with a pronounced right shoulder. This shoulder is a typical structure for liquid IV and III-V semiconductors, which are metallic in the melt. As we will show, superheated CdTe is metallic at 3000 K. For this temperature, the first peak, 1.9 Å, almost merges with the second peak. This is very different from supercooled CdTe, where the first and the second peaks become more pronounced and separated. The first peak moves to lower q, at 1.8 Å, while the second peak becomes asymmetric with a noticeable left shoulder.

We estimate the total and partial coordination numbers from the corresponding pair correlation functions as $C_{\alpha\beta}=\int_0^{R_{\min}}4\pi r^2 g_{\alpha\beta}(r)dr$. $R_{\min}$ is usually taken to be the first minimum in the total radial distribution function, $g(r)$, for the given temperature. Thus we take $R_{\min}=3.5$ Å, 3.6 Å, and 4.0Å for the supercooled, liquid, and superheated phases, respectively. To estimate quantitatively the concentration of the stoichiometry defects in the system, we introduce a compositional disorder number (CDN). This parameter is defined as a ratio of homogeneous to heterogeneous bond numbers: $(C_{\mathrm{CdCd}}+C_{\mathrm{TeTe}})/2C_{\mathrm{CdTe}}$. CDN can also be thought of as an order parameter. For instance, in the zinc-blende structure CDN is 0, whereas in a perfectly randomly mixed structure CDN is 1. In Table II, we present coordination numbers and CDNs at three different temperatures. For *l*-CdTe, the average number of neighbors in the first shell is 4.4. This indicates that CdTe retains its open structure upon melting. This is different from more close-packed liquid IV and III-V semiconductors, where the coordination number is ~6. However, upon further heating, CdTe transforms into a more close-packed phase with $C_{\mathrm{tot}}=6.5$. The CDN of *l*-CdTe is 0.4. This is in agreement with the assumption[20] that the dissociation degree of heterogeneous bonds in *l*-CdTe is noticeably smaller than in III-V compound melts. The structure of these melts is close to a random mix with CDN ~1.[18] Higher temperatures destroy stoichiometry order. Thus, for superheated CdTe, CDN is 0.8, approaching the random mix limit.

TABLE II. Total and partial coordination numbers for CdTe at three different temperatures.

	C_{tot}	C_{CdTe}	C_{CdCd}	C_{TeTe}	*CDN*
800	4.2	3.2	1.4	0.6	0.3
1370	4.4	3.3	1.5	0.9	0.4
3000	6.5	3.7	3.2	2.5	0.8

Partial pair correlation functions are presented in Fig. 5. For *l*-CdTe and supercooled CdTe, the correlation of the reference atom with the second shell is stronger than with the first one, in both g_{CdCd} and g_{TeTe} radial distributions. For superheated CdTe, temperature changes this correspondance between the first and second shells, making them comparable in weight. Clusters of Cd and Te retain some long-range structure, as the noticeable correlation in the third and even the fourth peaks indicates. The positions of the first two Te-Te shells are at ~2.9 Å and ~4.8 Å. This is opposite to the compact shells in Cd clusters with the positions at ~2.6 Å and ~4.0 Å.

In our simulations for *l*-CdTe, we observe that atoms of Te form branched chains. It is known that the trigonal phase of crystalline Te consists of close-packed infinite and parallel helicoidal chains. As experiment[34] and theoretical[35] studies suggest, Te also forms chainlike structures in the elemental liquid phase. It is interesting that this tendency of Te atoms to form chains is preserved in *l*-CdTe. More simple chains are present in supercooled CdTe.

It is useful to follow the behavior of the Te clusters as the temperature increases from 800 K to 3000 K. In our simulated supercooled CdTe, the Te chains are short with maximum length of three to four links. Only ~30% of Te atoms are bonded in these formations. As the temperature increases, the length of the chains increases. Te helicons become more irregular and ''twisted''; the chains start to ramify. At the melting temperature, there are Te filaments reaching the length of the whole supercell. Because of the imposed peri-

odicity of the system, some of the Te chains terminating at the opposite sides of the supercell become infinite. We find no Te triplets or tetrahedrons in the liquid. At 1370 K, 45% of Te atoms are bound with each other. As the temperatures grows further, the chains transform into more complex clusters with a higher coordination number $C_{\mathrm{TeTe}}=2.5$.

In Fig. 6, we illustrate configurations of Te clusters at different temperatures. To simplify the visualization of the plot, only atoms of Te are shown. Atoms are considered to be bonded if the distance between them is less than the first minimum, $R_{\min}$, of the total pair correlation function. The size of the cubic cell shown corresponds to $2\times2\times2$ supercell geometry. At 1370 K, infinite helicon chains can be seen in the figure.

Clusters of Cd have a different structure from the structure of Te chains in supercooled CdTe and *l*-CdTe. The difference corresponds to the fact that, for 800 K and 1370 K systems, the C_{CdCd} coordination numbers are larger (roughly by a factor of 2) than the C_{TeTe}. This implies a more close-packed structure of Cd clusters. Indeed, we find Cd clusters composed of tetrahedrons, triplets, and more complex rings in supercooled CdTe and *l*-CdTe. From the partial angular distribution of the bonds (Fig. 7), it can be seen that clusters of Te and Cd are drastically different for the 800 K system. The difference diminishes as the temperature increases. In the superheated state, it almost vanishes. The angle θ, corresponding to the open angle in the Te chains, dominates in the Te angular distribution. We find typically $\theta\sim160°$. At variance with the Te clusters, clusters of Cd have an angle $\theta\sim60°$ prevailing for supercooled CdTe. This angle represents the high concentration of triplets and close-packed Cd clusters. The total angular distribution is shown in Fig. 8. For superheated CdTe the $\sim60°$ angle dominates. As the temperature decreases, the tetrahedral angle starts to dominate.

B. Electronic properties

Once we know that the eigenpairs for a given atomic configuration are obtained, one can calculate the optical conductivity. According to the Kubo-Greenwood expression,[35] the real part of the conductivity can be expressed as

$$\sigma_r(\omega)=\frac{2\pi e^2}{3m^2\omega\Omega}\sum_{n,m}\sum_{\alpha=x,y,z}|\langle\psi_m|p_\alpha|\psi_n\rangle|^2\times\delta(E_n-E_m-\hbar\omega), \tag{4}$$

where E_i and ψ_i are eigenvalues and eigenfunctions, and Ω is the volume of the supercell. Dipole transition elements, $\langle\psi_m|p_\alpha|\psi_n\rangle$, were sampled by the Γ point of the BZ. The lowest 300 eigenstates are included in the summation. The real part of the optical conductivity of CdTe at different temperatures is displayed in Fig. 9. Each curve is the result of averaging several configurations chosen at random from the representative ensembles at each temperature. Typically, only five to ten configurations are required to obtain a converged conductivity. The dc conductivity value (at $\omega=0$) is linearly extrapolated from $\omega\to0$. According to our results, the dc conductivity is 0 for supercooled CdTe (the electron temperature in the Fermi-Dirac function was taken to be zero). At the melting temperature, CdTe experiences a semiconductor→semiconductor-type transition. Although

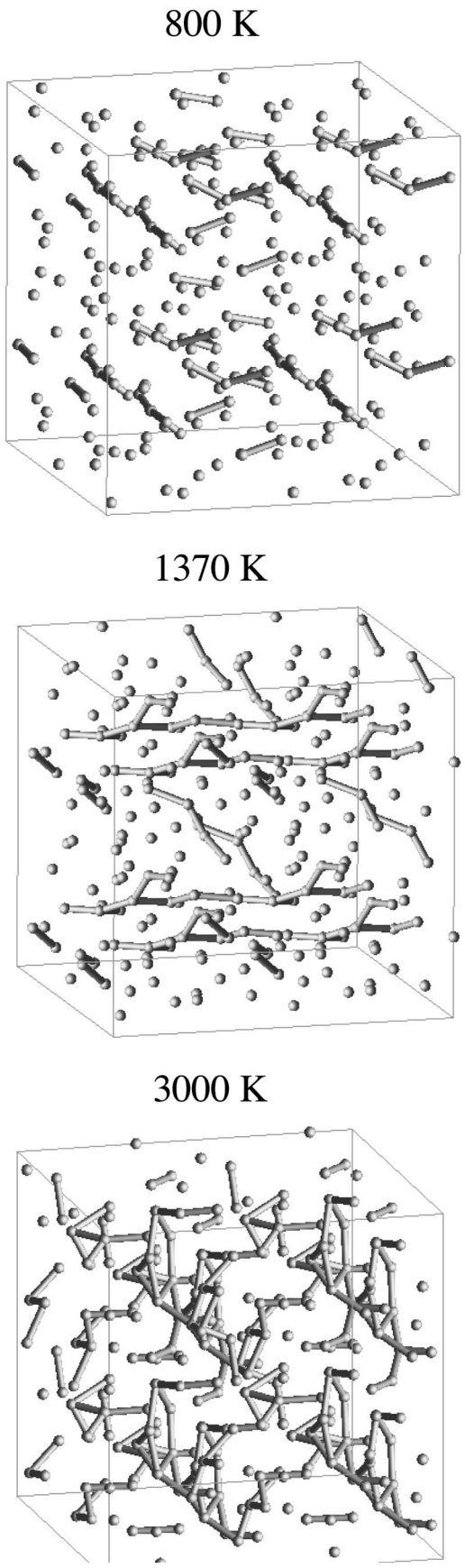

FIG. 6. Structure of liquid and amorphous CdTe. The boxes correspond to $2\times2\times2$ supercell geometry. Only atoms of Te and bonds between them are shown.

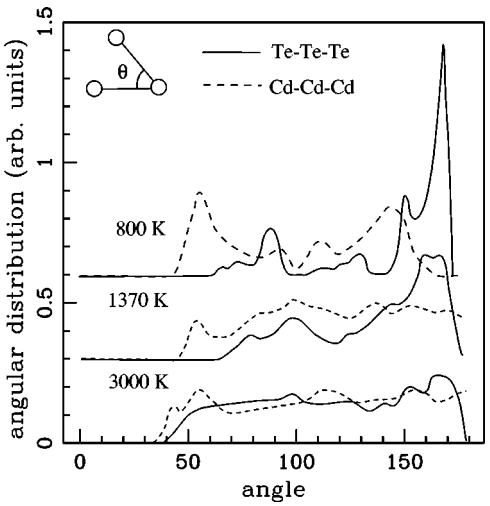

FIG. 7. Angular distribution of bond angles in Te and Cd clusters. The distribution is normalized by $\sin(\theta)$.

the electric conductivity of the melt increases by a factor of 40, the liquid remains a semiconductor as the conductivity increases upon further heating.[16] At ~120 degrees above the melting point, the conductivity appears to increase more rapidly.[16] The conventional interpretation is that at a high temperature CdTe undergoes a semiconductor→metal transition. However, we note that measuring the conductivity at, or above, the melting point is hindered by the high temperature and the jumplike increase of the conductivity. It is not surprising that experimental values for dc conductivity vary almost by a factor of 3 in the literature,[16,18,36] from 40 to 110 $\Omega^{-1}\,\mathrm{cm}^{-1}$. Our dc conductivity value is 100 $\Omega^{-1}\,\mathrm{cm}^{-1}$ at the melting temperature. Our value is in surprisingly good agreement with the experimental results. In particular, given our use of the Kohn-Sham eigenvalues, we do not expect an accurate representation of the excitation spectra.[37] Also, our temperature scale may not correspond precisely with experiment.

We find from our simulations that *l*-CdTe has a semiconductor-type conductivity: the real part of the conductivity does not have a metallic Drude-like dependence, $\sigma(\omega)\sim\sigma_0/(1+\omega^2\tau^2)$, on frequency as liquid IV and III-V semiconductors have.[1,6] The frequency-dependent conductivity for CdTe peaks at approximately 4 eV and then asymptotically goes to zero as $1/\omega^2$. Also, we find that in *l*-CdTe, the dc conductivity grows with the temperature. At 3000 K, the value of dc conductivity is 1000 $\Omega^{-1}\,\mathrm{cm}^{-1}$, an order of magnitude larger than the calculated value at the melting point.

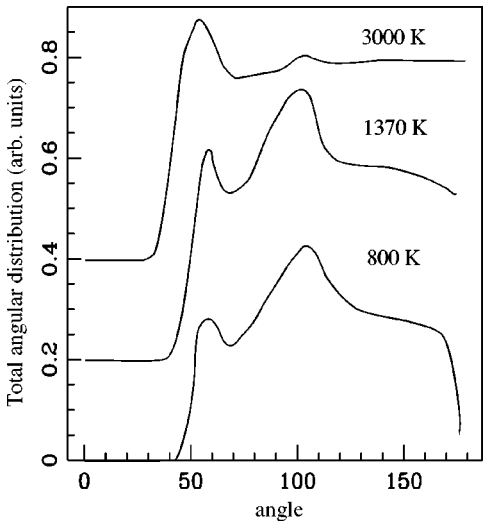

FIG. 8. Total angular distribution (in arbitrary units) of bond angles. The distribution is normalized by $\sin(\theta)$.

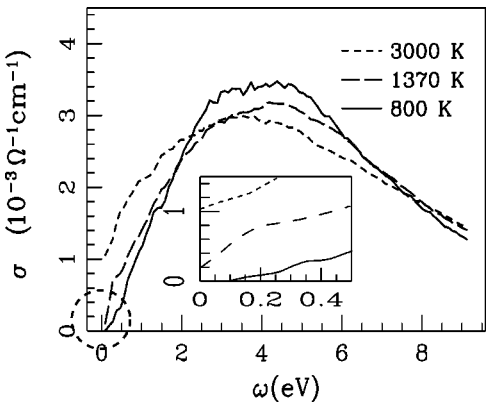

FIG. 9. Real part of optical conductivity. The circled area is enlarged and shown in the inset.

Temperature changes significantly alter the behavior of $\sigma(\omega)$ at small ω. To understand this behavior, we have examined how temperature affects the states near the Fermi level. The total and partial density-of-state functions (DOS)

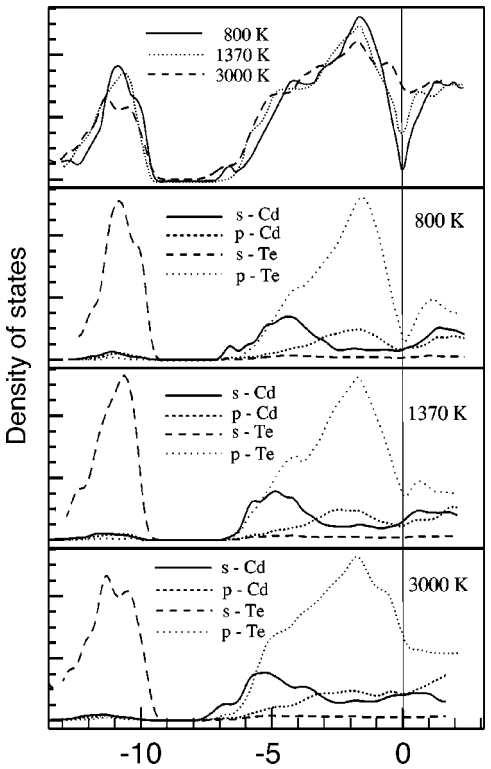

FIG. 10. Density-of-states functions. The upper panel represents total density of states of all valence electrons. The lower three panels represent partial density of states at 800 K, 1370 K, and 3000 K (only *s* and *p* projections of Cd and Te angular components are shown).

are displayed in Fig. 10. These curves are the result of averaging over ten atomic configurations taken at random from the corresponding ensemble at each temperature. To obtain partial the partial DOS functions, a Wigner-Seitz radius corresponding to one-half of the cell volume was used to deconvolve the wave function over spherical at harmonics around each atom. Each DOS is convoluted with 0.2 eV Gaussian (full width at half maximum). To preserve the sharp feartures of DOS at the Fermi level, the states near the Fermi level ($E_f \pm 0.5$ eV) are convoluted with 0.05 eV Gaussian. The transition between 0.2 eV and 0.05 eV Gaussians is peformed linearly in the energy intervals: $E_f - 1.0\,\text{eV} < E < E_f - 0.5\,\text{eV}$ and $E_f + 0.5\,\text{eV} < E < E_f + 1.0\,\text{eV}$.

At 800 K, there is a ''dip'' at the Fermi level. Since DOS is an average over a number of atomic configurations, where the Fermi energy has slightly different values, a well defined gap is not apparent in the DOS curve. Nonetheless, we find that the optical conductivity has a finite gap for small ω, at 800 K. There are several reasons for this ''paradox.'' First, at each time step a small gap can exist which is washed out in the averaging process. Also, even if the Fermi level resides between states whose energy separation is small, the dipole matrix elements between these states can vanish.

As the temperature increases, the band gap in the melt characterized by the DOS ''dip'' decreases quickly. The major contribution to the states which fill the gap comes from Te p electrons. At 3000 K, there is a higher concentration of Te-Te bonds and consequently Te clusters with higher coordination numbers. This is reflected in the splitting of the density-of-states contributions corresponding to Te s states into σ bonding and antibonding contributions. At higher temperatures, as the number of Te-Te bonds grows, the Te part of the DOS corresponding to p like states starts to resemble the elemental liquid Te valence DOS.[40] As in l-Te, the Te p-state contribution consists of σ and lone-pair (LP) states. As the number of Te-Te bonds increases, the LP contributions are affected by disorder. Various interactions with neighboring LP orbitals broaden the contributions to the DOS.[40] In superheated CdTe, the LP part of the DOS acquires a shoulder at -1 eV. In twofold-coordinated Te, the Fermi level is positioned between LP and antibonding σ^* states.[40] As the number of Te triplets and more complex clusters appear in the liquid, the LP contributions to the density of states become more than filled and the Fermi level moves in the antibonding σ^* contribution to the density of states, suggesting a semiconductor-to-metal transition. In l-Te, it also has been proposed[40] that it is the structure transformation from the pure chainlike configuration to the configuration with a limited number of Te triplets that induces the semiconductor→metal transition.

It is interesing to note that the peak of the conductivity occurs near $\hbar\omega = 4$ eV, independent of the melt temperatures investigated here. This is close to the ''average band gap'' in crystalline CdTe and likely represents a residual local order in the melt at the superheated temperature of 3000 K.

To quantify temperature changes in partial DOS functions, we integrate each curve representing a particular projected state up to the Fermi level (Table III). We chose to normalize the integrals to represent the number of electrons in the supercell having a particular angular character. There is no striking evidence in these calculations for electron delocalization with increasing temperature. Specifically, we expect that delocalization of the orbitals would result in an increase of the d- and f-state projections as a consequence of more ''free'' electronlike or metalliclike states. However, in our system, the total number of d and f electrons on either Cd and Te sites changes by less than 0.7 electrons as the systems goes from an amorphous to a superheated state. These d and f states are not localized in the band gap.

TABLE III. Sums of the numbers of states of different angular projections (see text).

	800 K	1370 K	3000 K
s-Te	58.7	59.3	60.8
p-Te	103.2	102.6	100.6
d-Te	4.2	4.5	5.8
f-Te	0.1	0.2	0.4
s-Cd	29.1	29.7	30.8
p-Cd	21.9	20.6	20.0
d-Cd	6.6	6.0	5.2
f-Cd	0.8	0.8	0.7

The primary change of the orbital character in the melt is the redistribution of s and p electrons as the temperature grows. The number of s electrons increases on both Cd and Te sites, while the number of p electrons decreases. We attribute this process to the relaxation of sp-hybridized electrons as the number of like-atom bonds increases with the temperature. Overall, we would characterize the semiconductor→metal transition as being caused by a change of the electronic states at the Fermi level, while the rest of the states are not altered dramatically.

C. Dynamic properties

By following the atomic positions in the liquid state as a function of time, we can calculate the diffusion of Cd and Te in l-CdTe. For this calculation, we set the Langevin viscosity paramter to zero and follow the trajectories of each atom in the liquid. The diffusion constant can be determined as $D = \lim_{t\to\infty}(\langle[R(t)]^2\rangle/6t)$. The mean-square displacement is given by $\langle[R(t)]^2\rangle = (1/N)\sum_{i=1}^{N}[R_i(t) - R_i(0)]^2$. $R_i(t)$ is the position of the ith atom. The average is over all the atoms, N, in the unit cell. Our results for the diffusion coefficients are given in Table IV. We were able to find only the diffusion coefficient of Te in l-CdTe. Agreement of our data with the available experiment is very good. In Fig. 11, we show the behavior of the diffusion coefficients as functions of time and temperature during annealing of l-CdTe to 800 K. Diffusivity values of both Cd and Te decrease by a factor

TABLE IV. Diffusion coefficients of Cd and Te in l-CdTe and superheated-CdTe.

	D_{Cd} (10^{-5} cm^2 s^{-1})	D_{Te} (10^{-5} cm^2 s^{-1})
1370 K (theory)	6.7	5.2
1370 K (experiment) (Ref. 18)		5.0
3000 K (theory)	8.6	6.7

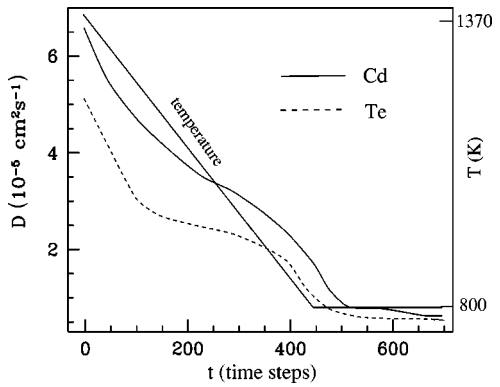

FIG. 11. Time dependence of the diffusion coefficients as *l*-CdTe is annealed from 1370 K to 800 K to obtain supercooled-CdTe. Temperature beahavior is marked on the right.

of magnitude as we supercool the liquid. Diffusion coefficients drop to $D_{Cd}=7.2\times10^{-6}\,\mathrm{cm^2\,s^{-1}}$ and $D_{\mathrm{Te}}=6.0\times10^{-6}\,\mathrm{cm^2\,s^{-1}}$.

IV. CONCLUSION

We performed *ab initio* molecular-dynamics simulation of CdTe at three different temperatures. Our theoretical results for *l*-CdTe are in good agreement with available experimental data: structure factor, diffusion coefficient, and dc conductivity. In agreement with experiment,[9] *l*-CdTe retains its open structure with the coordination number ~4 upon melting. This is different from liquid IV and III–V semiconductors, where the coordination number is ~6. Also, in the molten state, CdTe has a smaller dissociation degree than molten IV and III-V semiconductors that have more random structure. The composition disorder number (CDN), defined as the ratio of the homogeneous to heterogeneous bonds, is 0.4 in *l*-CdTe. Further heating leads to significant structural changes of the liquid. Thus, in superheated CdTe, the coordination number increases to 6.5. Also, the higher CDN value of 0.8 reveals a more randomly mixed structure.

We find that in contrast to III-V (or IV) semiconductors, CdTe experiences a semiconductor→semiconductor transition upon melting. We attribute this to the higher ionicity of bonds in CdTe and the corresponding structural differences in the melt. In the liquid IV or III-V semiconductors, entropy favors a disordered and close-packed structure. As a result, a transition occurs from a fourfold structure to a more randomly mixed and a denser sixfold-coordinated structure. In *l*-CdTe, the higher ionicity of anion-cation bonds does not favor a proximity of like atoms. We believe that this limits the miscibility of different types of atoms and causes long-range correlation in partial radial distributions for like atoms. As a result, the internal energy term in the free energy prevents the entropy term from inducing a transition to a more close-packed and randomly mixed phase. The higher ionicity of Cd-Te bonds also limits the delocalization of electrons, which contributes to the semiconductor properties of *l*-CdTe.

While at the melting temperature, *l*-CdTe is a semiconductor (with the dc conductivity growing as the temperature increases), further heating causes a sharp increase of the electrical conductivity and semiconductor→metal transition. In our simulations we observed that electrical conductivity grows with the temperature. Thus dc conductivity at 3000 K is larger by an order of magnitude than the value at the melting temperature. We found that at all three temperatures, the CdTe system has a strong ionic character without any significant delocalization of electron wave functions. Further metallization of the melt is not caused by the introduction of free electrons in the system as covalent bonds break, as in the case of liquid IV and III-V semiconductors. Metallic bahavior of liquid CdTe is induced by the structural changes. As more Te-Te bonds are created in the system and more complex and disordered Te clusters appear, a finite number of Te *p* states appear at the Fermi level. While the density of states of supercooled CdTe has a well defined dip at the Fermi energy, it disappears as the temperature grows.

In *l*-CdTe at the melting temperature, atoms of Te form infinite branched chains, typical for pure liquid Te. As the temperature increases, the chains disrupt and transform in more complex and close-packed clusters with higher coordination numbers. We were able to observe the Te filaments in the supercooled liquid, though the chains were shorter and less ramified than at the melting temperature.

ACKNOWLEDGMENTS

This work was funded in part by Grant No. NASA/NAG8-1258 from the Micogravity Materials Science program of the National Aeronautics and Space Administration. Also, we would like to acknowledge support for this work by the NSF and by the Minnesota Supercomputer Institute. One of us (J.R.C.) would like to thank the Miller Institute for its support.

[1] I. Stich, R. Car, and M. Parrinello, Phys. Rev. B **44**, 4262 (1991).
[2] P. Silvestrelli, A. Alavi, M. Parrinello, and D. Frenkel, Phys. Rev. Lett. **77**, 3149 (1996).
[3] G. Kresse and J. Hafner, Phys. Rev. B **49**, 14 251 (1994).
[4] V. Godlevsky, J. R. Chelikowsky, and N. Troullier, Phys. Rev. B **52**, 13 281 (1995).
[5] I. Lee and K. Chang, Phys. Rev. B **50**, 18 083 (1994).
[6] Q. Zhang, G. Chiarotti, A. Selloni, R. Car, and M. Parrinello, Phys. Rev. B **42**, 5071 (1990).
[7] C. Molteni, L. Colombo, and L. Miglio, J. Phys.: Condens. Matter **6**, 5255 (1994).
[8] L. Lewis, A. De Vita, and R. Car, Phys. Rev. B **57**, 1594 (1998).
[9] J. Gaspard, C. Bergman, C. Bichara, R. Bellissent, P. Chieux, and J. Coffard, J. Non-Cryst. Solids **97/98**, 1283 (1987).
[10] J. Gaspard, J. Raty, R. Ceolin, and R. Bellissent, J. Non-Cryst. Solids **205–207**, 75 (1996).
[11] K. Zanio, Semicond. Semimet. **13**, (1978).
[12] P. Rudolph and M. Muhlberg, Mater. Sci. Eng., B **16**, 8 (1993).
[13] D. J. Larson, Micrograviy News **1(6)**, 10 (Winter 1994).
[14] Preliminary results on conductivity differences between CdTe and GaAs may be found in V. Godlevsky, J. Derby, and J. R. Chelikowsky, Phys. Rev. Lett. **81**, 4959 (1998).

[15] A. Joffe and A. Regel, *Progress in Semiconductors* (Heywood, London, 1960), Vol. 4, p. 237.
[16] V. Glazov, S. Chizhevskaya, and N. Glagoleva, *Liquid Semiconductors* (Plenum, New York, 1969).
[17] G. Kresse and J. Hafner, Phys. Rev. B **55**, 7539 (1997).
[18] P. Rudolph, Prog. Cryst. Growth Charact. **29**, 275 (1994).
[19] P. Kröger, *The Chemistry of Imperfect Crystals* (American Elsevier Comp., New York, 1973), Vol. 1, p. 195.
[20] M. Jordan, Metall. Trans. A **1**, 239 (1970).
[21] V. Godlevsky and J. R. Chelikowsky, J. Chem. Phys. **108**, 7312 (1998).
[22] B. Lichter and P. Sommelet, Trans. AIME **245**, 1021 (1969).
[23] S. Louie, S. Froyen, and M. Cohen, Phys. Rev. B **26**, 1738 (1982).
[24] N. Troullier and J. L. Martins, Phys. Rev. B **43**, 1993 (1991).
[25] D. M. Ceperley and B. J. Alder, Phys. Rev. Lett. **45**, 566 (1980).
[26] L. Kleinman and D. Bylander, Phys. Rev. Lett. **48**, 1425 (1982).
[27] R. Biswas and D. Hamann, Phys. Rev. B **34**, 895 (1986).
[28] N. Binggeli, J. L. Martins, and J. R. Chelikowsky, Phys. Rev. Lett. **68**, 2956 (1992).
[29] J. Q. Broughton and X. P. Li, Phys. Rev. B **35**, 9120 (1987).
[30] O. Sugino and R. Car, Phys. Rev. Lett. **74**, 1823 (1995).
[31] G. Phillips, *Bands and Bonds in Semiconductors* (Academic Press, New York, 1973).
[32] J. Emsley, *The Elements*, 3rd ed. (Oxford University Press, Oxford, UK, 1996).
[33] V. Glazov and L. Pavlova, J. Cryst. Growth **184/185**, 1253 (1998).
[34] M. Yao and H. Endo, J. Non-Cryst. Solids **205–207**, 85 (1996).
[35] R. Kubo, J. Phys. Soc. Jpn. **12**, 570 (1957); D. Greenwood, Proc. Phys. Soc. London **71**, 585 (1958).
[36] L. Shcherbak, J. Cryst. Growth **184/185**, 1057 (1998).
[37] M. Hybertsen and S. Louie, Phys. Rev. B **38**, 4033 (1988).
[38] H. McShimin and D. Thomas, J. Appl. Phys. **33**, 56 (1962).
[39] D. Berlincourt, H. Jaffe, and L. Shiozawa, Phys. Rev. **129**, 1009 (1963).
[40] C. Bichara, J. Raty, and J. Gaspard, J. Non-Cryst. Solids **205–207**, 361 (1996).